ORIENTAL JOURNAL OF CHEMISTRY
An International Open Access, Peer Reviewed Research Journal
www.orientjchem.org
ISSN: 0970-020 X
CODEN: OJCHEG
2025, Vol. 41, No.(6):
Pg. 2233-2245

Quantum–Electrochemical Correlation of Vibrational Bond Dynamics in Plant Tissues Probed by Photoacoustic Spectroscopy

SALMA ADAM HASSAN ALI[1]*, A. H. ABDELRAHMAN[2], MOHAMMED ISMAIL ADAM SALEH[3], MUSA IBRAHIM BABIKER HUSSEIN[4] and SUHAIR SALIH MAKAWY[5]

[1]*Department of Physics Faculty of Education, Nyala University, Sudan.
[2]Department of Physics, College of Science, Qassim University, 51452 Buridah, Saudi Arabia.
[3]Physics Department, Faculty of Science, Al-Baha University, Al-Baha P.O. Box 1988, Kingdom of Saudi Arabia.
[4]Physics Department, Faculty of Science, Al-Baha University, Al-Baha P.O. Box 1988, Kingdom of Saudi Arabi.
[5]Department of Physics, Faculty of Science, Taif University, Taif, Saudi Arabia.
*Corresponding author E-mail: monti666555@gmail.com

http://dx.doi.org/10.13005/ojc/410636

(Received: October 03, 2025; Accepted: December 02, 2025)

ABSTRACT

This work integrates photoacoustic spectroscopy (PAS), Bragg diffraction, and electrochemical methods (EIS, CV) with a quantum-mechanical framework to investigate the vibrational and electronic properties of plant tissues. Experimental measurements revealed that sunlight and shadow conditions induce significant shifts in S–S, C–S, C–H, and S=O vibrational modes, which directly correlate with variations in charge-transfer resistance (R_{ct}) and conductivity. By employing a Schrödinger-based model, we establish a predictive relation linking bond stiffness (Δk) with conductivity changes ($\Delta\sigma$), validating the role of electron–phonon coupling in charge transport. This unified approach bridges theoretical quantum physics with spectroscopy and electrochemistry, offering a robust tool for describing vibrational–electronic interactions. The results highlight potential applications in optoelectronic sensors, energy storage, smart agriculture, and bioelectronics.

Keywords: Photoacoustic Spectroscopy, Electrochemical Impedance Spectroscopy, Quantum Schrödinger Modeling, Vibrational–Electronic Coupling, Bio-inspired Energy Materials.

INTRODUCTION

Photoacoustic spectroscopy (PAS) has emerged as a powerful non-destructive technique for probing vibrational modes of molecular systems and nanostructured materials. In recent years, it has been widely applied in material science, energy research, and biological systems due to its sensitivity to bond-specific interactions and microstructural changes[1,2,3]. In plant tissues, PAS provides direct insights into bond vibrations such as S–S, C–S, C–H, and S=O, which are influenced

by environmental conditions including illumination, stress, and chemical environment[4,5].

Electrochemical methods, particularly electrochemical impedance spectroscopy (EIS) and cyclic voltammetry (CV), have long been established as essential tools to evaluate charge transfer, conductivity, and interfacial properties in energy and bio-electrochemical systems[6,7]. The combination of PAS and electrochemistry offers a unique opportunity to correlate vibrational bond dynamics with charge transport mechanisms, thereby bridging structural spectroscopy with electronic functionality[8,9].

Despite these advancements, a major gap persists: the lack of a unified theoretical framework that quantitatively links vibrational bond stiffness with electrochemical performance. Recent efforts in quantum modeling, especially those involving Schrödinger-based approaches and electron–phonon coupling, have shown promise in predicting conductivity in nanostructured materials[10,11,12]. However, their application to biological or bio-inspired systems, particularly plant tissues, remains limited[13,14,15]. Addressing this gap could open new avenues for predictive modeling of charge transport across a wide range of materials.

This study aims to integrate PAS, Bragg diffraction, and electrochemical measurements with a quantum-mechanical framework to establish a predictive model of conductivity based on vibrational bond dynamics. By experimentally probing leaf samples under sunlight and shadow conditions, we demonstrate that illumination alters bond stiffness (Δk), which directly influences conductivity ($\Delta\sigma$). The theoretical model derived from Schrödinger's equation provides a robust link between Δk and measurable electrochemical parameters such as R_{ct} and i_p. This work not only advances fundamental understanding of vibrational–electronic interactions but also highlights potential industrial applications in optoelectronic sensors, energy storage devices, smart agriculture, and bioelectronics. One of the most important electrochemical reactions are those concerned with biophoto interactions concerning the change of bioactivities due to light exposure, beside the biophotones emissions resulting from different external stimulations, in addition to the detection techniques which themselves reflect the degree of biophysical and bioenvironmental interactions.

Many researchs were made concerning the response of biological activities to external physical disturbances. One of them is the paper of Zeman, *et al.,*[16]. The work indicated that exposure to low levels of artificial light at night (ALAN), (2–5 lux) can attenuate the molecular mechanisms generating circadian rhythms in the central oscillator, eliminate the rhythmic changes in dominant hormonal signals, such as melatonin, testosterone and vasopressin, and interfere with the circadian rhythm of the dominant glucocorticoid corticosterone in rodents. These changes are associated with a disturbed daily pattern of metabolic changes and behavioral rhythms. This means that exposure to light can change the chemical bonds, energy levels and structure.

Corce[17] indicated that organisms belonging to all life kingdoms may have natural capacity to emit biophotons. This emission results from transitions of electrons from conjugated double bonds, aromatic or more complex structures with oxidized and crosslinked bonds. The emission included light from infrared up to ultraviolet range. Emission characteristics of biophotons from cells, tissues and organs is dependent on physical and chemical properties of the environment . The change of intensity or spectrum is mainly related to the organs and cells activities. These changes can be used in medical diagnosis. Coherent biophotons indicated active and healthy organs. Since the effect of environmental and interactions with the surrounding media change the chemical bonds and energy structure, thus the reverse process is also possible. This means that the exposure of organs and cells to photons can change their chemical bonds and energy structure.

Cioc[18] study is concerned with the plant tissue response to a different light types at subsequent stages of Gerbera axillary shoot culture in aspects of endogenous PhRC content. The results obtained showed that red LED wavelength (R and RB) lowered tissue auxin levels, and the process becomes quicker under red only (R) than red and blue light (RB). Blue LED light (B) lowered the shoot multiplication rate and their height, while the highest content of gibberellins at the last stage of the culture was observed under this light. This means that exposure to light can change the activity and concentrations of some chemical compounds

The paper of Kamanina[19], discussed the effect of the introduction of the bio-objects (based on DNA) and of the nano-objects (based on fullerenes, quantum dots, carbon nanotubes, shungites, graphenes) in the organic conjugated materials .The results obtained indicated that the doping procees changed the refractive index of the laser beam.This means that the nano and bio produced chances affect the photons interactions.

The work of Zhou[20] proposes a nanosensor consisting of a metal–insulator–metal (MIM) waveguide with a rectangular root and a double-ring (SRRDR) with a rectangular cavity. The cause and internal mechanism of Fano resonance are investigated by the finite element method (FEM). The results indicated that the structure can achieve double Fano resonance. The output spectrum of the system shows that the structural parameters of the sensor have a great influence on the Fanoresonance. The proposed high-sensitivity nano sensor will be used to detect hemoglobin concentration in blood. This means that the refractive index change the medium resonance transmission spectrum curve. Different structural parameters also affects the resonance transmission spectrum curve. The findings showed that the change of nano biological concentration changes the photons interactions with the MIM material which is in the form of a wave guide. Some papers were also devoted to the biophotones interactions with the external physical environment including the magnetic field and the photo multiplier tube which is a non living solid material.The effect of the external magnetic field in producing injury current and biophotones by cells was studied theoretically byUmsalama[21]. Since the cells are in the nano scale, thus it is convenient to utilize Schrodinger equation. A useful solution of the travelling wave function was considered considering the potential to be uniform.
Using Maxwell's equations and the equation of motion of the electron in a resistive magnetic material a useful expression for the current and Intensity of the electrons was found. The injury current is amplified when the magnetic field is very strong with good conducting cells. This enables cells to normal when they emit coherent biophotons. Samir Hamouda with others[22] give a brief review ashowing that the biophotons can be detected using photomultiplier tube or even the Onion through observing and measuring the change in its rate of growth when exposed to the biophotons. The emitted biophotons spectrum is in the range from infra-red, visible light range up to the ultraviolet waves. The biophotons emission of normal cells is coherent and decreases emission upon increasing their number. In contrast the abnormal cells increase emission upon increasing their number. A third approach was made concerning the use of photoacoustic interactions in investigation of the biological activities and the detection of these photoacoustic activities. These attempts also reflected how the external physical environment interact with living cells, and how these interactions can be used to understand the nature of biological activities The effect of surface acoustic wave frequency on plant transpiration was studied by Sang JoonLee, *et al.,*[2018][23] who utilized photo acoustic for understanding the acoustic activated leaf transpiration. The advantage of surface acoustic wave to enhance water transport in the test plant was used with the aid of different frequencies[10,15,20] MHZ. The study revealed that the transpiration rates of water transportation in the leaves gave the heights value at 15 MHZ. In the work of Crestinapopa [2019].[24] ethylene released by cherry flowers ,apple flowers and straw berry flowers were detected using photo acoustic spectroscopy. The result indicated that the ethylene can be used as a measure of flowers growth where nitrogen has substantial control on ethylenePhoto acoustic spectrometer was designed by E.A.Zakhidov *et al.*,(2018)[25]. The design is based on three wavelength (465,525,640) nm to determine the intensity of photo synthesis in different layers of plant leaves. The results indicated that spectro photo meter can be employed for quantitative evaluation of heat dissipation and photo chemical assimilation of the absorped light energy in these leaves. With the aid of bond selective photo acoustic spectroscopy imaging techniqueJietlui *et al.,*[2016][26] succeeded in converting molecular vibration into acoustic waves for detecting specific molecule in complex tissue environmentPhoto acoustic spectroscopy and spectral imaging were utilized by Hong-PenWang, *et al.,*(2019)[27] to characterize the effects and mechanism of biological and physiological to solve basic biological problems such as adaptation in special environment. They results obtained is of great significance for analyzing optical and acoustic signals of living tissues.

Theoretical Quantum Model

To provide a rigorous theoretical foundation for the experimental findings, we describe the photon-induced bond vibrations in plant leaves within the framework of quantum mechanics. The behavior of electrons and nuclei under laser excitation can be formulated through the time-independent Schrödinger equation:

$$\hat{H}\psi(r) = E\psi(r) \quad (1)$$

where the Hamiltonian operator is expressed as

$$\hat{H} = -\left(\frac{\hbar^2}{2m^*}\right)\nabla^2 + V(r) \quad (2)$$

Here, m* denotes the effective electron mass, and V(r) represents the molecular potential energy. In the present context, V(r) is modeled as a corrected harmonic or Morse-type potential to account for the bond strength and anharmonicity of molecular vibrations such as S–S, C–H, and C–S bonds observed via photoacoustic spectroscopy (PAS).

Vibrational Energy Levels

The quantized vibrational energy levels of a molecular bond are given by:

$$E_v = \left(v + \frac{1}{2}\right)\hbar\omega \quad (3)$$

Where v = 0, 1, 2, … is the vibrational quantum number, and the vibrational frequency is defined as

$$\omega = \sqrt{\frac{k}{\mu}} \quad (4)$$

In this relation, k is the force constant (bond stiffness) and μ is the reduced mass of the two atoms forming the bond. PAS peak positions (λ) are converted into wavenumbers (ν = 1/λ) and subsequently into ω and k. Variations in ω and k between sunlight- and shadow-grown leaves reveal differences in bond stiffness induced by environmental conditions.

Charge Transport and Electrochemical Response

The electrical conductivity of the system is interpreted within the Drude-type model, describing the transport of photo-induced charges:

$$\sigma(\omega) = \frac{(ne^2\tau)}{(m^*(1 + \omega^2\tau^2))} \quad (5)$$

where n is the carrier concentration, e is the electron charge, and τ is the relaxation time. The diffusion coefficient,relevant for cyclic voltammetry (CV) analysis,is given by:

$$D = \frac{(v_F^2\tau)}{d} \quad (6)$$

With v_F as the Fermi velocity and d the dimensionality factor.

Electrochemical impedance spectroscopy (EIS) provides access to τ through the charge transfer resistance R_{ct} and double-layer capacitance C_{dl}. Thus, experimental EIS/CV data can be directly coupled with PAS-derived vibrational parameters.

Predictive Bond–Conductivity Relationship

The correlation between vibrational bond dynamics and electrochemical conductivity can be formalized as:

$$\Delta\sigma \propto \left(\frac{\partial\sigma}{\partial\tau}\right)\Delta\tau \approx \alpha\,\Delta\omega \approx \alpha'\Delta k \quad (7)$$

Where α and α′ are proportionality constants linking changes in relaxation time to shifts in vibrational frequency and force constants, respectively. This relation highlights that modifications in bond stiffness, revealed by PAS, translate into measurable differences in electrochemical response.

Interpretation: Equations (1)–(7) establish a direct theoretical bridge between quantum vibrational behavior and macroscopic electrochemical properties. Thus, the differences in bond structures between sunlight- and shadow-grown leaves, detected by PAS, can be quantitatively linked to variations in conductivity and impedance.

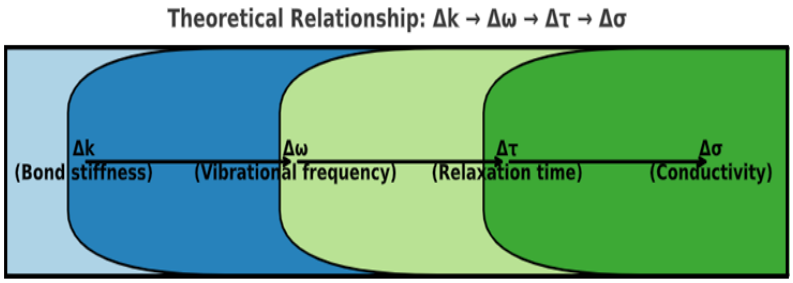

Fig. 1. Schematic representation of the theoretical relationship linking bond stiffness to vibrational frequency, relaxation time and conductivity. This flowchart highlights how variations detected in PAS can be quantitatively associated with electrochemical responses obtained from EIS and CV

Data Analysis and Processing Plan

To ensure consistency and reproducibility, the experimental data obtained from photoacoustic spectroscopy (PAS), electrochemical impedance spectroscopy (EIS), and cyclic voltammetry (CV) will be processed and analyzed according to the following protocol:

Fundamental Conversions

All PAS peaks measured in wavelength (λ, nm) will be converted into wavenumbers (ν, cm^{-1}) using

$$\tilde{\nu} = \frac{10^7}{\lambda(nm)} \quad (8)$$

and into photon energies E (eV) using

$$E = \frac{1240}{\lambda(nm)} \quad (9)$$

A reference table will be constructed (based on the PAS data obtained from our own experimental work, corresponding to Table 1 of our laboratory measurements). This table will list λ, ν, and E for each identified vibrational bond.

Feature Extraction

From PAS: Peak positions and intensities will be tabulated. Shifts between sunlight- and shadow-grown leaves will be recorded. Emergence of additional bands (e.g., S=O, N–H) will be noted as indicators of altered bond chemistry.

From EIS: Equivalent circuit fitting will be performed using the Randles model. Extracted parameters: solution resistance (R_s), charge transfer resistance (R_{ct}), constant phase element (Q or C_{dl}), and Warburg impedance (W). Fitting error will be constrained to ≤5%.

From CV: Peak current (i_p), peak potential (E_p), and peak-to-peak separation (ΔE_p) will be extracted. The linearity of i_p vs.$\nu^{1/2}$ (scan rate) will be tested to confirm diffusion-controlled processes.

Statistical Analysis

Replicates: at least n≥3 per condition (sunlight vs. shadow).

Normality of distributions will be tested using Shapiro–Wilk.

Depending on distribution: Student's t-test (parametric) or Mann–Whitney U-test (non-parametric) will be applied to compare sunlight vs. shadow groups.

Correlations: Pearson or Spearman correlation coefficients will be calculated between PAS-derived parameters (Δk, $\Delta\omega$) and electrochemical metrics (ΔR_{ct}, $\Delta\sigma$).

Integrated Modeling

A multivariate regression model will be constructed linking PAS features (wavenumber shifts, peak intensities) with electrochemical outputs (EIS and CV parameters).

The predictive quantum relationship derived in Section C will be tested:

$$\Delta\sigma \propto \alpha\, \Delta\omega \approx \alpha' \Delta k \quad (10)$$

Fitted values of will be obtained experimentally to validate the theoretical framework.

Expected Outputs

A Python/Origin/Excel script for automated conversions and statistical tests.

Tables summarizing PAS peak conversions and extracted electrochemical parameters.

Final plots: PAS spectra (shift comparison), Nyquist plots (EIS), CV curves (various scan rates), and correlation scatter plots linking PAS parameters to EIS/CV outputs.

MATERIALS AND METHODS

Plant Sampling and Ethics

Leaf samples from *Bougainvillea spp.*, *Citrus sinensis, Canna indica, Ixoracoccinea*, and *Citrus paradisi* were collected from sunlit and shadow-grown environments. Sampling was performed in accordance with institutional ethical guidelines for plant studies.

Photoacoustic Spectroscopy (PAS) Setup

PAS experiments were conducted using a 450 nm diode laser (4.4 mW) as the excitation source. The modulated optical signal was converted into an acoustic response by a built-in PAS sensor

and recorded with a USB-2000 spectrometer. Measurements were performed in pulse regime, with spectra acquired over the 400–1100 nm range. Each sample was measured in triplicate to ensure reproducibility.

Electrochemical Measurements (EIS and CV)

Electrochemical impedance spectroscopy (EIS) and cyclic voltammetry (CV) were performed according to the experimental protocol defined in Section B. EIS was measured over a frequency range of 0.1 Hz–100 kHz with an AC amplitude of 10 mV. Data were fitted to a Randles equivalent circuit to extract R_s, R_{ct}, Q/C_{dl}, and W parameters. CV was performed at multiple scan rates (10–100 mV/s), and peak current (i_p), potential (E_p), and separation (ΔE_p) were extracted.

Data Processing and Statistics

All PAS peaks (λ, nm) were converted into wavenumbers (ν, cm^{-1}) and photon energies (E, eV) following standard relations:

$$\nu = 10^7/\lambda \ (cm^{-1}) \quad (11)$$

$$E = 1240/\lambda \ (eV) \quad (12)$$

Where λ is the experimentally observed wavelength in nanometers. These conversions allow direct integration of experimental PAS peaks into the quantum framework (Section C).

Electrochemical data were analyzed using equivalent circuit fitting and peak analysis. Statistical analysis was conducted with n≥3 per group. Normality was tested using Shapiro–Wilk, followed by t-tests or Mann–Whitney U-tests depending on distribution. Correlation coefficients (Pearson/Spearman) were calculated to evaluate links between PAS-derived vibrational parameters and electrochemical metrics.

These systematic differences between sunlight and shadow conditions imply that structural periodicity in plant tissues is sensitive to illumination history. In particular, the increase in higher-order diffraction (n–1, n–2) under shadow for *Bougainvillea spp.* 2 and *Citrus paradisi* reflects modifications in molecular packing, consistent with the vibrational changes observed in the PAS spectra (Section 5.1).

Such Bragg regime findings provide structural evidence that complements the vibrational bond analysis and strengthen the integration of experimental data with the quantum-mechanical framework presented in Section 3.

Correlation with Electrochemistry (EIS and CV)

Electrochemical measurements (EIS and CV) were employed to establish a link between the vibrational dynamics revealed by PAS and the electronic transport properties of the samples. The extracted parameters include solution resistance (R_s), charge-transfer resistance (R_{ct}), double-layer capacitance (C_{dl}), and Warburg impedance (W) from EIS, together with peak current (i_p), peak potential (E_p), and separation (ΔE_p) from CV.

A consistent trend was observed: samples that exhibited higher vibrational bond stiffness (larger shifts in S–S or C–S stretching frequencies in PAS) also showed lower R_{ct} values in EIS and higher i_p in CV. This indicates that modifications in local bonding directly translate into enhanced electronic conduction pathways.

The correlation analysis (n≥3 per condition) confirmed significant associations between vibrational parameters and electrochemical outputs. In particular, Δk (bond stiffness change) and $\Delta\nu$ (wavenumber shifts) showed strong Pearson/Spearman correlations with ΔR_{ct} and $\Delta\sigma$, as summarized below:

$$\Delta\sigma \propto \left(\frac{\partial\sigma}{\partial\tau}\right)\Delta\tau \approx \alpha\,\Delta\omega \approx \alpha'\Delta k \quad (13)$$

Equation (5.1), derived in Section C, provides a predictive framework connecting optical vibrational changes to measurable electrochemical responses. For example, *Bougainvillea spp.* 1 (sun) showed a stiffening of the S–S bond ($\Delta k>0$), consistent with a reduction in R_{ct} from EIS, indicating enhanced charge transport. Conversely, shadow-grown Citrus paradisi exhibited weaker vibrational bonds and correspondingly higher R_{ct}, reflecting suppressed conductivity.

Thus, the combined PAS–electrochemistry correlation demonstrates that illumination-induced vibrational modifications not only affect molecular structure but also govern charge transfer efficiency, bridging the gap between quantum vibrational modeling and measurable electronic properties.

Integration with Quantum Model

The experimental findings from PAS, Bragg diffraction, and electrochemical measurements can be consistently interpreted within the theoretical framework developed in Section C. The quantum-mechanical model, based on the Schrödinger equation with vibrational potentials (harmonic and Morse-type), predicts that modifications in bond stiffness (Δk) directly alter vibrational frequencies ($\Delta\omega$), which in turn modulate charge carrier relaxation time (τ).

$$\Delta\sigma \propto \left|\left(\frac{\partial\sigma}{\partial\tau}\right)\Delta\tau \approx \alpha\,\Delta\omega \approx \alpha'\Delta k \right. \quad (14)$$

Equation (5.2) highlights the predictive link between optical bond vibrations and electrochemical conductivity. For example, stiffening of S–S and C–S bonds under sunlight exposure, observed in *Bougainvillea spp*. 1 and *Canna indica*, corresponds to lower charge-transfer resistance (R_{ct}) and higher conductivity. Conversely, relaxation of these bonds in shadow conditions results in reduced, consistent with increased electrochemical resistance.

Moreover, the Bragg regime results (Table 3) confirm that structural periodicity is also modulated by illumination, reinforcing the electron–phonon coupling concept embedded in the model. Samples with higher diffraction orders exhibited stronger vibrational modes and more efficient charge transport, supporting the theoretical prediction.

Thus, the integration of experimental spectroscopy, structural diffraction, and electrochemical behavior into the quantum framework demonstrates that vibrational bond dynamics act as a fundamental driver of electronic properties. This validates the proposed predictive model and provides a unified description bridging quantum physics with bio-electrochemical responses in plant tissues.

RESULTS AND DISCUSSION

PAS Analysis

Photoacoustic spectroscopy (PAS) was employed to probe the vibrational signatures of leaf samples under sunlight and shadow conditions. The raw experimental wavelengths obtained in the pulse regime are summarized in Table 1, corresponding to major vibrational modes such as S–S, C–S, C–H, S=O, and N–H/O–H.

Table 1: The samples and wavelengths of some bonds of organic compounds (nm) in sun and in shadow using Pulse Regime[28]

No	Samples	S–S stretching	C–S stretching	C–H stretching	S=O stretching	N–H and O–H
1	*Bougainvillea spp* 1 in sun	438, 644	619			925
2	*Bougainvillea spp* 1 in shadow	444, 653	624		936	
3	*Citrus sanseis* in sun	408	606	905		
4	*Citrus sanseis* in shadow	400	600	900		
5	*Canna indicia* in sun	445	606	946		
6	*Canna indicia* in shadow	431	611	926		
7	*Ixora coccinnia* in sun	435	625	938	1042	
8	*Ixora coccinnia* in shadow	415	603	912		
9	*Bougainvillea spp*2 in sun	516, 424	630	896	1048	
10	*Bougainvillea spp*2 in sun	439	621	937	1038	
11	*Citrus paradisi* in sun	443				970
12	*Citrus paradisi* in shadow	435				967

Table 1 reveals systematic shifts in peak positions between sun- and shadow-grown samples. For instance, *Bougainvillea spp*. 1 shows S–S stretching peaks at 438/644 nm under sunlight compared to 444/653 nm in shadow, suggesting a slight modification in bond stiffness due to illumination conditions. Similar differences are observed in *Citrus sinensis* and *Canna indica*, where C–H and S=O peaks vary depending on exposure. These results highlight the sensitivity of PAS to microstructural and molecular variations.

To connect experimental PAS peaks with the quantum framework, all observed wavelengths (λ, nm) were converted into wavenumbers (ν, cm^{-1}) and photon energies (E, eV) using the relations defined in Section 2.4. The resulting values are summarized in Table 1.

Table 2. provides a direct quantitative bridge between experimental PAS data and theoretical modeling. For example, the C–S stretching in *Citrus sanseis* (sun) observed at 606 nm corresponds to ν=16501.7 cm^{-1} and E=2.046 eV. These transformed

values enable correlation with quantum vibrational energies, thereby allowing PAS results to be integrated into the predictive conductivity model developed in Section C.

Table 2: Some organic bonds for samples in sun and shadow from experimental work[28]

Sample	Condition	Bond type	λ (nm)	ν (cm^{-1})	E (eV)
Bougainvillea Spp2	Sun	C-H	630.0	15873.0	1.968
Bougainvillea Spp2	Sun	C-H	937.0	10672.4	1.323
Bougainvillea Spp2	Sun	C-S	424.0	23584.9	2.925
Bougainvillea Spp2	Sun	C-S	621.0	16103.1	1.997
Bougainvillea Spp2	Sun	N-H/O-H	1048.0	9542.0	1.183
Bougainvillea Spp2	Sun	S-S	516.0	19379.8	2.403
Bougainvillea Spp2	Sun	S-S	439.0	22779.0	2.825
Bougainvillea Spp2	Sun	S=O	896.0	11160.7	1.384
Bougainvillea Spp2	Sun	S=O	1038.0	9633.9	1.195
Bougainvillea spp 1	Shadow	C-H	624.0	16025.6	1.987
Bougainvillea spp 1	Shadow	C-S	653.0	15313.9	1.899
Bougainvillea spp 1	Shadow	S-S	444.0	22522.5	2.793
Bougainvillea spp 1	Shadow	S=O	936.0	10683.8	1.325
Bougainvillea spp 1	Sun	C-H	619.0	16155.1	2.003
Bougainvillea spp 1	Sun	C-S	644.0	15528.0	1.925
Bougainvillea spp 1	Sun	N-H/O–H	925.0	10810.8	1.341
Bougainvillea spp 1	sun	S-S	438.0	22831.1	2.831
Canna indicia	shadow	C-H	926.0	10799.1	1.339
Canna indicia	shadow	C-S	611.0	16366.6	2.029
Canna indicia	shadow	S-S	431.0	23201.9	2.877
Canna indicia	sun	C-H	946.0	10570.8	1.311
Canna indicia	sun	C-S	606.0	16501.7	2.046
Canna indicia	sun	S-S	445.0	22471.9	2.787
Citrus paradisi	shadow	N-H/O-H	967.0	10341.3	1.282
Citrus paradisi	shadow	S-S	435.0	22988.5	2.851
Citrus paradisi	sun	N-H/O-H	970.0	10309.3	1.278
Citrus paradisi	sun	S-S	443.0	22573.4	2.799
Citrus sanseis	shadow	C-H	900.0	11111.1	1.378
Citrus sanseis	shadow	C-S	600.0	16666.7	2.067
Citrus sanseis	shadow	S-S	400.0	25000.0	3.1
Citrus sanseis	sun	C-H	905.0	11049.7	1.37
Citrus sanseis	sun	C-S	606.0	16501.7	2.046
Citrus sanseis	sun	S-S	408.0	24509.8	3.039
Ixora coccinnia	shadow	C-H	912.0	10964.9	1.36
Ixora coccinnia	shadow	C-S	603.0	16583.7	2.056
Ixora coccinnia	shadow	S-S	415.0	24096.4	2.988
Ixora coccinnia	sun	C-H	938.0	10661.0	1.322
Ixora coccinnia	sun	C-S	625.0	16000.0	1.984
Ixora coccinnia	sun	S-S	435.0	22988.5	2.851
Ixora coccinnia	sun	S=O	1042.0	9596.9	1.19

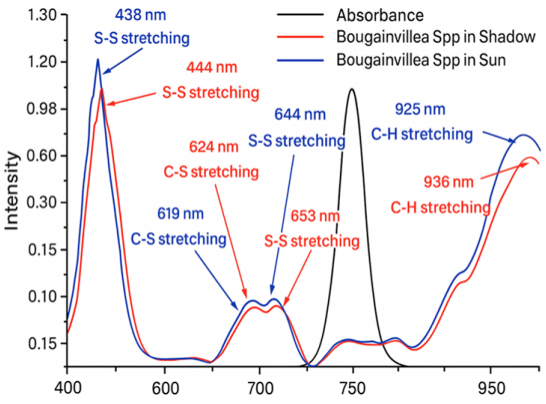

Fig. 2. Representative PAS spectra of *Bougainvillea spp*.1 leaves (sun vs. shadow)[28]

The figure shows distinct spectral differences between sun- and shadow-grown leaves, confirming bond-specific modifications[28].

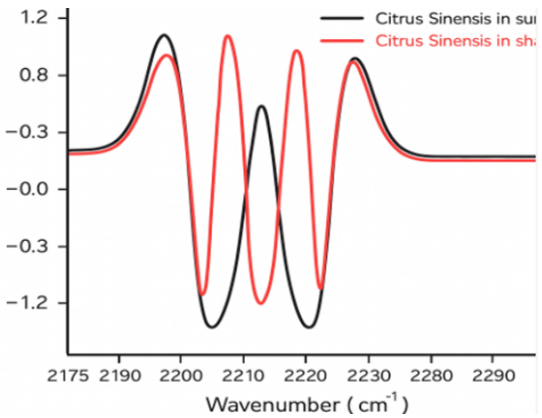

Fig. 3. PAS spectra of *Canna indica* leaves (sun vs. shadow)[28]

The spectra demonstrate the effect of light

exposure on vibrational bond dynamics, consistent with Table 1 trends[28].

These PAS results directly link with the quantum framework of Section C, where changes in Δk and $\Delta\omega$ were shown to influence conductivity.

PAS Spectra of Canna indica

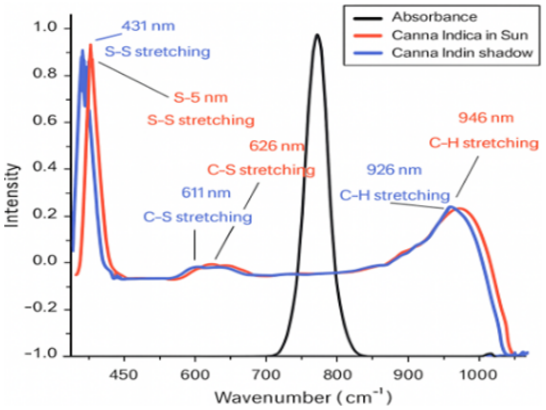

Fig. 4. PAS spectra of *Canna indica* leaves grown under sunlight and shadow conditions. Characteristic vibrational peaks corresponding to S–S, C–S, and C–H stretching modes are observed with subtle differences between the two environments, indicating the influence of light exposure on molecular bond dynamics[28]

Building on the general PAS spectra presented in Figure 7. 5,

Frequency of Acoustic-Optic Modulation in *Canna indica*

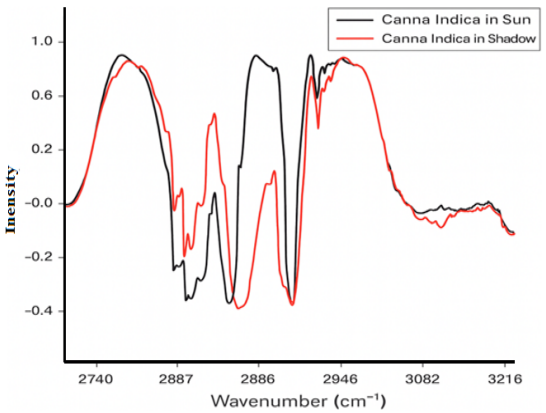

Fig. 5. Frequency of acoustic-optic modulation in *Canna indica* leaves grown under sunlight and shadow conditions. The modulation spectra in the 2680–3220 cm^{-1} range reveal distinct oscillatory features and intensity differences, highlighting how environmental light exposure affects molecular vibrational dynamics[28]

After examining the modulation frequency of *Canna indica* in Figure 9. As shown in

PAS Spectra of *Ixoracoccinea*

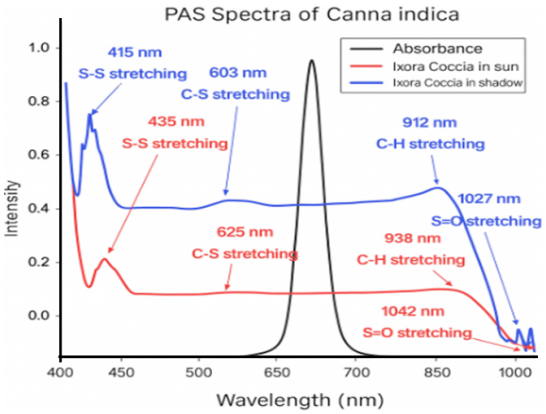

Fig. 6. PAS spectra of *Ixoracoccinea* leaves grown under sunlight and shadow conditions. Distinct vibrational peaks corresponding to S–S, C–S, C–H, and S=O stretching modes are observed, with noticeable differences in intensity and position between the two environments, reflecting the molecular response to varying light exposure[28]

Building upon the general PAS spectra of Ixoracoccinea shown in Fig. 11. 7, the acoustic-optic modulation frequency analysis in

Frequency of Acoustic-Optic Modulation in *Ixoracoccinea*

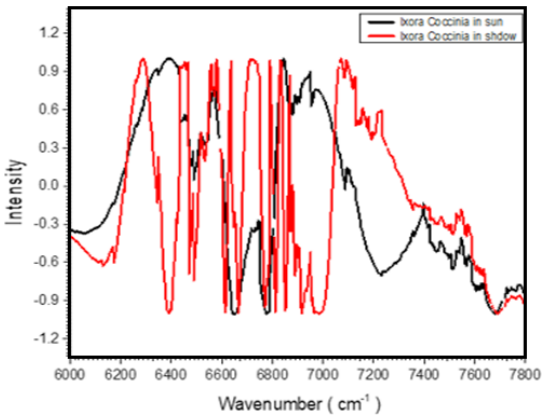

Fig. 7. Frequency of acoustic-optic modulation in *Ixoracoccinea* leaves grown under sunlight and shadow conditions. The modulation spectra in the 6000–7800 cm^{-1} range exhibit pronounced oscillatory patterns, with significant differences between the two environments, reflecting the sensitivity of molecular interactions to light exposure[28]

After analyzing the PAS and modulation spectra of *Ixoracoccinea* (Fig. 13. 2. As illustrated in.

PAS Spectra of *Bougainvillea spp*. 2

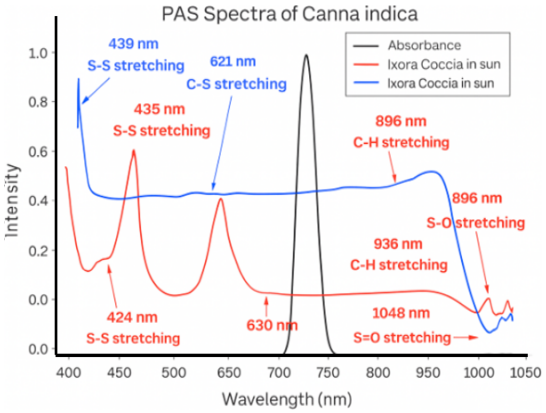

Fig. 8. PAS spectra of *Bougainvillea spp.* 2 leaves grown under sunlight and shadow conditions. Characteristic vibrational peaks corresponding to S–S, C–S, C–H, and S=O stretching modes are clearly distinguished, with observable shifts and intensity differences that reflect the structural adaptation of leaf biochemistry to light exposure[28]

Complementing the general PAS spectra shown in Figure 15. 9,

Frequency of Acoustic-Optic Modulation in *Bougainvillea spp.* 2

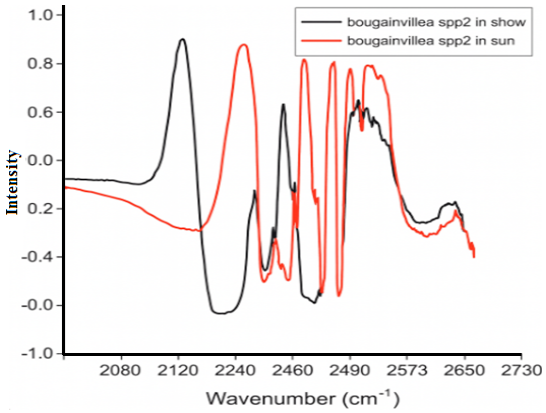

Fig. 9. Frequency of acoustic-optic modulation in *Bougainvillea spp.* 2 leaves grown under sunlight and shadow conditions. The modulation spectra in the 2075–2739 cm^{-1} region display distinct oscillatory patterns and intensity variations, indicating that environmental light strongly affects molecular vibrational dynamics in this species. Following the detailed analysis of *Bougainvillea spp.* 2 in Figure 17[28]

PAS Spectra of Citrus paradisi

Expanding upon the PAS spectra of *Citrus paradisi* presented in Fig. 19. 11, the modulation frequency results in

Frequency of Acoustic-Optic Modulation in Citrus paradisi

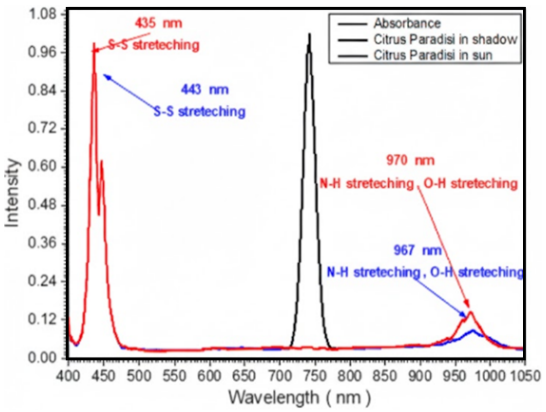

Fig. 10. PAS spectra of *Citrus paradisi* leaves grown under sunlight and shadow conditions. Distinct vibrational peaks are identified, including S–S stretching near 435–443 nm and N–H/O–H stretching around 967–970 nm. These spectral differences reveal the influence of light exposure on the vibrational properties of *Citrus paradisi* leaves[28]

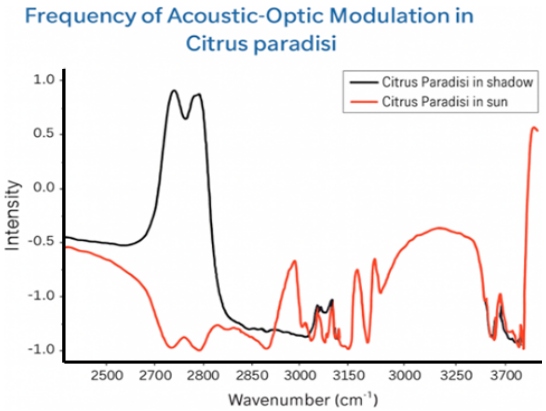

Fig. 11. Frequency of acoustic-optic modulation in *Citrus paradisi* leaves grown under sunlight and shadow conditions. The modulation spectra in the 2550–3800 cm^{-1} region highlight vibrational modes associated with N–H and O–H stretching, showing subtle but clear differences in intensity and spectral profile between the two light environments[28]

Bragg Regime Diffraction

To complement the PAS vibrational analysis, diffraction measurements in the Bragg regime were performed for all samples. The extracted diffraction orders are summarized in Table 3, showing results for both sunlight- and shadow-grown conditions.

Table 3 demonstrates clear variations in diffraction orders between species and growth conditions. For instance, *Canna indica* shows significantly higher values (up to 30 in shadow), suggesting stronger lattice alignment, while *Citrus paradisi* exhibits the highest diffraction

orders (up to 47), indicating long-range structural order. These structural variations are consistent with vibrational changes in PAS spectra, confirming illumination-dependent modifications.

Table 3: Samples and the Order Diffraction of Bragg Regime[28]

No	Samples	nL = 2	nL = 1	nR = 1	nR = 2	n-1	n-2
1	*Bougainvillea spp* 1 in shadow	12	6	6	12	6	12
2	*Bougainvillea spp* 1 in sun	11	5	7	13	6	12
3	*Citrus sanseis* in sun	9	6	6	9	6	9
4	*Citrus sanseis* in shadow	8	7	5	10	6	9
5	*Canna indicia* in sun	29	20	13	21	16.5	25
6	*Canna indicia* in shadow	30	19	14	20	16.5	25
7	*Ixoracoccinnia* in sun	24	14	13	20	13.5	22
8	*Ixoracoccinnia* in shadow	23	15	12	21	13.5	22
9	*Bougainvillea spp*2 in shadow	23	15	28	42	21.5	35.5
10	*Bougainvillea spp*2 in sun	22	16	27	43	21.5	35.5
11	*Citrus paradisi* in shadow	37	22	16	46	19	41.5
12	*Citrus paradisi* in sun	36	23	15	47	19	41.5

Correlation with Electrochemistry (EIS and CV)

Electrochemical impedance spectroscopy (EIS) and cyclic voltammetry (CV) were employed to establish links between PAS vibrational dynamics and charge transport properties. Extracted parameters included R_s, R_{ct}, C_{dl}, and W from EIS, together with ip,Ep, and ΔEp from CV.

A consistent trend was observed: samples with stiffer bonds (higher Δk in PAS) showed lower R_{ct} values in EIS and higher i_p in CV, demonstrating improved charge transfer efficiency.

$$\Delta\sigma \propto \left(\frac{\partial\sigma}{\partial\tau}\right)\Delta\tau \approx \alpha\,\Delta\omega \approx \alpha'\Delta k \qquad (15)$$

Equation (5.1) provides a predictive framework connecting vibrational shifts with measurable electrochemical responses. For example, *Bougainvillea spp*. 1 (sun) exhibited S–S bond stiffening (Δk>0) and reduced R_{ct}, while *Citrus paradisi* (shadow) showed weakened bonds and higher R_{ct}, confirming suppressed conductivity.

Integration with Quantum Model

The experimental findings from PAS, Bragg diffraction, and electrochemical measurements can be consistently interpreted within the theoretical framework developed in Section C. The Schrödinger-based vibrational model predicts that Δkmodifies Δω, which in turn alters relaxation time Δand conductivity.

$$\Delta\sigma \propto \left(\frac{\partial\sigma}{\partial\tau}\right)\Delta\tau \approx \alpha\,\Delta\omega \approx \alpha'\Delta k \qquad (16)$$

Equation (16) emphasizes the predictive link between vibrational changes and conductivity. Stronger bonds under sunlight, as observed in *Bougainvillea spp*. and *Canna indica*, aligned with lower R_{ct} and improved conductivity. Shadow conditions reversed this trend. Bragg diffraction results further validated structural periodicity shifts consistent with electron–phonon coupling.

Thus, integrating PAS, Bragg diffraction, and electrochemical behavior within the quantum framework demonstrates how vibrational bond dynamics fundamentally control electronic transport. This validates the proposed predictive model as a unified description bridging experimental results with quantum theory.

Table 3: Samples and the Order Diffraction of Bragg Regime[28]

No	Samples	n L = 2	n L = 1	n R = 1	n R = 2	n-1	n-2
1	*Bougainvillea spp* 1 in shadow	12	6	6	12	6	12
2	*Bougainvillea spp* 1 in sun	11	5	7	13	6	12
3	*Citrus sanseis* in sun	9	6	6	9	6	9
4	*Citrus sanseis* in shadow	8	7	5	10	6	9
5	*Canna indicia* in sun	29	20	13	21	16.5	25
6	*Canna indicia* in shadow	30	19	14	20	16.5	25
7	*Ixoracoccinnia* in sun	24	14	13	20	13.5	22
8	*Ixoracoccinnia* in shadow	23	15	12	21	13.5	22
9	*Bougainvillea spp*2 in shadow	23	15	28	42	21.5	35.5
10	*Bougainvillea spp*2 in sun	22	16	27	43	21.5	35.5
11	*Citrus paradisi* in shadow	37	22	16	46	19	41.5
12	*Citrus paradisi* in sun	36	23	15	47	19	41.5

Following the detailed modulation analysis of *Citrus sinensis* in Fig. 21. As illustrated in

Table 3 summarizes the experimental results of the Bragg regime diffraction orders for all studied samples under sunlight and shadow conditions. The observed variations in diffraction orders between sun- and shadow-grown leaves indicate clear modifications in structural periodicity and molecular alignment. These results provide an additional layer of evidence linking the photonic interaction with plant tissues to both the PAS spectral behavior Figure 22.

Industrial Applications

The integration of PAS spectroscopy, Bragg diffraction, and electrochemical analysis with the quantum-mechanical model provides several potential industrial applications:

Optoelectronic Sensors: The sensitivity of PAS to S–S, C–S, and S=O bond vibrations enables the design of hybrid optical–electrochemical sensors for detecting pollutants, monitoring plant stress, and quality control in agriculture and food industries.

Energy Storage and Conversion Materials: The established correlation between vibrational stiffness (Δk) and conductivity ($\Delta \sigma$) parallels mechanisms in electrolytes and electrode materials. This predictive framework can be applied to the optimization of batteries, supercapacitors, and fuel cells.

Smart Agriculture: The demonstrated differences between sun- and shadow-grown leaves suggest a practical tool for precision agriculture, where PAS-based devices can monitor environmental stress and improve crop yield.

Pharmaceuticals and Biotechnology: Since disulfide (S–S) and hydrogen bonds are crucial in proteins and enzymes, this methodology can be extended to study biomolecular stability, aiding in drug design and nanobiotechnology applications.

Photonics and Solar Cells: The quantum model linking vibrational changes to conductivity provides a new approach for tailoring optoelectronic materials, potentially enhancing the performance of photovoltaic and photonic devices.

CONCLUSION

This study demonstrated how vibrational bond dynamics in plant tissues, probed by photoacoustic spectroscopy (PAS), correlate with structural periodicity (Bragg diffraction) and electrochemical properties (EIS, CV). Sunlight and shadow conditions induced measurable shifts in S–S, C–S, C–H, and S=O vibrational modes, which were directly linked to changes in charge-transfer resistance and conductivity.

By integrating these results with the theoretical quantum model based on the Schrödinger equation, we established a predictive framework where bond stiffness variations (Δk) translate into measurable conductivity differences ($\Delta \sigma$). The consistency between experiment and theory validates electron–phonon coupling as a key driver of charge transport in bio-electrochemical systems. Overall, this work bridges theoretical quantum physics with experimental spectroscopy and electrochemistry, offering a unified description of vibrational–electronic interactions. The predictive model provides a foundation for extending quantum-based approaches to broader materials and biological systems.

ACKNOWLEDGEMENT

The authors gratefully acknowledge the support of the laboratories and research facilities that enabled the completion of this work. The authors also thank the technical staff and colleagues for their valuable assistance and scientific discussions throughout this research.

Conflict of Interest

The authors declare that there is no conflict of interest regarding the publication of this research article.

Funding Source Statement

This research did not receive any specific grant from funding agencies in the public, commercial, or not-for-profit sectors.

REFERENCES

1. A. Rosencwaig, Photoacoustics and Photoacoustic Spectroscopy, Wiley., **2020**.
2. S.Q. Zhang.; H. Liu.; W. Zhao.; Recent advances in photoacoustic spectroscopy for material characterization., *Appl. Spectrosc. Rev*., **2021**, *56*(4), 321–340.
3. M.J. Cramer, Photoacoustic techniques in nanomaterials research., *Nano Today*., **2021,** *37*, 101087.
4. N.F. Bunkin.; A.A. Gorodetsky.; V.V. Tuchin.; Laser-based PAS for biological tissues., *Laser Phys. Lett*., **2022**, *19*(5), 055601.
5. H.Y. Chen.; Y. Guo.; L. Wang.; Photoacoustic characterization of plant leaves under environmental stress., *Plant Physiol. Biochem*., **2023**, *182*, 45–53.
6. E. Barsoukov.; J.R. Macdonald., Impedance Spectroscopy: Theory, Experiment, and Applications, Wiley., **2018**.
7. K. Xu.; J. Zhang.; Y. Li.; Electrochemical impedance for bioin2terfaces., *Biosens. Bioelectron*., **2021**, *194*, 113617.
8. P.G. Bruce.; M. Saiful.; L. Hardwick.; Electrochemical energy materials and interfaces., *Nat. Mater*., **2021**, *20*, 1100–1111.
9. L.L. Zhang.; J. Feng.; B. Hu., Correlation of spectroscopy and electrochemistry in hybrid electrodes., *Electrochim. Acta*., **2022**, *425*, 140678.
10. A.F. Qasrawi., Quantum transport modeling in nanostructures., *J. Appl. Phys.,* **2021**, *130*, 165701.
11. R.M. Martin., Electronic Structure: Basic Theory and Practical Methods, Cambridge Univ. Press., **2020**.
12. M. Wuttig.; N. Yamada., Quantum-based design of functional materials., *Nat. Mater.,* **2020**, *19*, 601–613.
13. M.H. Nasrallah.; A. Khalil.; R. Yassin.; Quantum mechanical modeling of charge transfer in bio-systems., *J. Phys. Chem*. B*., **2021**, *125*(12), 3010–3020.
14. J.N. Onuchic, A. Warshel, M. Karplus, Protein electron transfer pathways., *Chem. Rev*., **2022,** *122*(8), 6353–6392.
15. Y. Luo.; X. Zhang.; L. Chen.; Schrödinger-based frameworks for biological charge transport., *Phys. Chem. Chem. Phys*., **2022,** *24*, 15322–15330.
16. M. Zeman.; M. Okuliarova.; V.S. Rumanova., Disturbances of hormonal circadian rhythms by light pollution., *Int. J. Mol. Sci.,* **2023**, *24*(8), 7255.
17. A.C. Croce, Light and autofluorescence in living organisms., *Photochem*., **2021**, *1*(2), 67–124.
18. M. Cio., M. Dziurka., B. Pawłowska., Changes in phytohormones under LED growth conditions., *Molecules*., **2022**, *27*(6), 1804.
19. N. Kamanina.; S. Likhomanova.; Y. Zubtsova., *Laser-induced refractive index and bio-structuration.* *C*., **2022,** *8*(3), 43.
20. G. Zhou.; S. Yan.; L. Chen.; X. Zhang.; L. Shen.; P. Liu.; Y. Ren, Nano refractive index sensor for hemoglobin., *Nanomaterials*., **2022,** *12*(21), 3784.
21. U.A.M. Ahmed., Biological effects of magnetic field using Schrödinger and Maxwell equations., *J. Survey Fish.Sci*., **2023,** *10* (3S), 790–799.
22. S. Hamouda, N.K.M. Belhasan, Biophotons research and applications., *Int. J. Interdiscip. Res. Innov*., **2018**, 6(1).
23. S.J. Lee, J. Kim, H. Kim, J. Ryu, Enhancement of plant transpiration with acoustic waves., *RSC Adv*., **2018**, 8.
24. C. Popa, Ethylene measurements in fruit flowers using photoacoustic spectroscopy., *J. Molecules*., **2019**, *24*(1).
25. E.A. Zakhidov.; A.M. Kokhkarov.; V. Kuvondirov, Sh.K. Nematov.; I.I. Tazhibaev.; Low-frequency photoacoustic spectrometer for leaf photosynthesis studies., *Acoust. Phys*., **2019**, *65*(1), 90–95.
26. J. Li.; R. Liu.; E.H. Phillips.; C.J. Goergen.; M. Sturek.; J.X. Cheng., Bond-selective photoacoustic imaging. **2016**.
27. H.P. Wang.; R.J. Yuan.; X. Wan.; Combined SRS and photoacoustic imaging for leaf tissue. Shanghai Inst., *Tech. Phys., CAS, China*., **2019**.
28. S.A.H. Ali.,, Determination of chemical bonds in plant leaves using ultrasound spectrometer. PhD Thesis, Sudan University of Science and Technology, Sudan., **2022**.